Neuron
Article

Adaptation to Background Light Enables Contrast Coding at Rod Bipolar Cell Synapses

Jiang-Bin Ke,[1,7] Yanbin V. Wang,[2,3,7] Bart G. Borghuis,[3] Mark S. Cembrowski,[4] Hermann Riecke,[5] William L. Kath,[5,6] Jonathan B. Demb,[2,3,*] and Joshua H. Singer[1,*]
[1]Department of Biology, University of Maryland, College Park, MD 20742, USA
[2]Department of Cellular and Molecular Physiology
[3]Department of Ophthalmology and Visual Science
Yale University, New Haven, CT 06511, USA
[4]Howard Hughes Medical Institute, Janelia Farm Research Campus, Ashburn, VA 20147, USA
[5]Department of Engineering Sciences and Applied Mathematics
[6]Department of Neurobiology and Physiology
Northwestern University, Evanston, IL 60208, USA
[7]These authors contributed equally to this work
*Correspondence: jonathan.demb@yale.edu (J.B.D.), jhsinger@umd.edu (J.H.S.)
http://dx.doi.org/10.1016/j.neuron.2013.10.054

SUMMARY

Rod photoreceptors contribute to vision over an ~6-log-unit range of light intensities. The wide dynamic range of rod vision is thought to depend upon light intensity-dependent switching between two parallel pathways linking rods to ganglion cells: a rod→rod bipolar (RB) cell pathway that operates at dim backgrounds and a rod→cone→cone bipolar cell pathway that operates at brighter backgrounds. We evaluated this conventional model of rod vision by recording rod-mediated light responses from ganglion and AII amacrine cells and by recording RB-mediated synaptic currents from AII amacrine cells in mouse retina. Contrary to the conventional model, we found that the RB pathway functioned at backgrounds sufficient to activate the rod→cone pathway. As background light intensity increased, the RB's role changed from encoding the absorption of single photons to encoding contrast modulations around mean luminance. This transition is explained by the intrinsic dynamics of transmission from RB synapses.

INTRODUCTION

In mammalian retina, cones—the photoreceptors that mediate daylight vision—signal to ganglion cells (GCs) through ~12 types of cone bipolar (CB) cells (Masland, 2012; Wässle et al., 2009). ON CBs and OFF CBs are depolarized by increments and decrements in light intensity and contact ON and OFF GCs, respectively. By contrast, rods—the photoreceptors that mediate night vision—signal to GCs by three distinct pathways, all of which "piggyback" on the cone circuitry (Demb and Singer, 2012; Strettoi et al., 1992) (Figure 1). The first and most sensitive is the rod bipolar (RB) cell pathway, in which rod signals are conveyed to RBs and then to CBs and GCs via AII amacrine cells. In the second pathway, rods signal to cones through gap junctions and thereby directly modulate cone→CB synapses. In the third pathway, rods make synapses with a subset of OFF CBs and thereby influence a few OFF GC types (Arman and Sampath, 2012; DeVries and Baylor, 1995; Mataruga et al., 2007; Protti et al., 2005; Soucy et al., 1998; Tsukamoto et al., 2001).

Although the basic anatomy of rod circuits is established (Figure 1), we lack a clear description of each circuit's function. There is evidence that the RB pathway saturates at moderate backgrounds and loses its ability to signal: backgrounds evoking ~10–100 rhodopsin isomerizations (R*)/rod/s reduce the sensitivity of the RB pathway by >90% (Dunn et al., 2006; Oesch and Diamond, 2011). The paradigms that established the sensitivity of this and other rod pathways, however, relied on brief flashes of light imposed on a background (i.e., Weber contrast) rather than modulation of intensity—comprising both increments and decrements—around a background (i.e., Michelson contrast). We reasoned that because reductions in RB gain are attributable to synaptic depression at RB synapses (Dunn and Rieke, 2008; Jarsky et al., 2011; Oesch et al., 2011), stimuli that included decrements (i.e., negative contrast) should be encoded even at relatively high backgrounds. This is because decrements should hyperpolarize RBs, suppress release, and thereby permit recovery from synaptic depression.

In the experiments that follow, we reevaluated the hypothesis that the rod→RB pathway is utilized for signaling exclusively near visual threshold. We found that for >1 log unit of intensity and in the absence of direct cone stimulation, the RB pathway operated in parallel with the rod→cone pathway to encode contrast around the mean luminance. A transition in the RB's role with light intensity, from encoding single-photon absorptions to encoding contrast, could be explained by the intrinsic dynamics of transmission from RB synapses.

RESULTS

Background Light Eliminates Event Detection in the RB Pathway

To assess event detection in rod pathways, we recorded responses in ON and OFF GCs evoked by dim 10 ms flashes

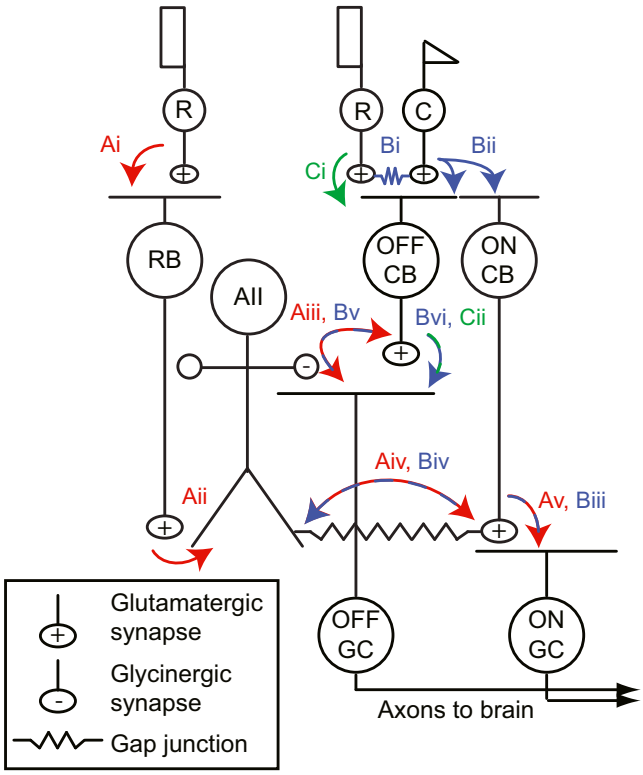

Figure 1. Rod Pathways in the Mammalian Retina

(Ai–Av) In red: the rod bipolar (RB) pathway. Rods make synapses onto RBs (Ai), which make synapses onto AIIs (Aii). AIIs make glycinergic synapses (Aiii) onto the terminals of some OFF cone bipolar (CB) cells and onto the dendrites of some OFF ganglion cells (GCs). AIIs are coupled by electrical synapses to the terminals of ON CBs (Aiv), which make glutamatergic synapses onto ON GCs (Av). The AMPAR antagonist DNQX blocks transmission from RBs to AIIs (Aii). (Bi–Bvi) In blue: rods are coupled electrically to cones by gap junctions (Bi), and cones make synapses onto ON and OFF CBs (Bii). Depolarization of the ON CB by the cone not only drives glutamatergic transmission to ON GCs (Biii), it also depolarizes AIIs via the electrical synapse (Biv) and thereby elicits glycinergic transmission to OFF GCs and, perhaps, OFF CBs (Bv). Signaling from cones to OFF GCs via the AII (Bi→Bii→Biv→Bv) is preserved in the presence of DNQX. OFF CBs make glutamatergic synapses onto OFF GCs (Bvi).

(Ci and Cii) In green: rods make direct chemical synapses onto some types of OFF CB (Ci), which in turn contact OFF GCs (Cii). Transmission through this pathway is blocked by DNQX.

in the ventral mouse retina, where rods could be stimulated selectively by green light (Wang et al., 2011; see below). Excitatory currents (I_{exc}; V_{hold} = −70 mV) were recorded from ON Alpha GCs and inhibitory currents (I_{inh}; V_{hold} = 0 mV) from OFF Alpha and Delta GCs (OFF T and S cells, respectively [Margolis and Detwiler, 2007; Murphy and Rieke, 2006, 2008; Pang et al., 2007; van Wyk et al., 2009]).

Both ON and OFF GCs exhibited half-maximal responses to flashes evoking 0.1–0.3 R*/rod (Figures 2A and 2B). Here, sensitivity might have been affected adversely by incomplete dark adaptation and, in some cases, by recording from multiple cells in the same tissue preparation (see Experimental Procedures). Nevertheless, sensitivity was within the expected range, and it was reduced by >95% when the flashes were imposed on a background of 100 R*/rod/s (Figures 2A and 2B), consistent with published results (Dunn et al., 2006; Murphy and Rieke, 2008). Responses to dim flashes (0.1 R*/rod) were suppressed throughout exposure to the background (30 s) (Figure 2C1), even though there was some recovery of the baseline current measured between flashes (Figure 2C2). When the background was turned off, flash responses recovered in ~10 s (Figure 2C1). This experiment confirmed GCs' pronounced and persistent insensitivity to dim flashes in the presence of moderate background light.

The measured flash responses could be mediated by either the rod→RB or the rod→cone pathway or by some combination of the two. To differentiate the contributions of the two pathways, we blocked the rod→RB pathway with the AMPA/kainate receptor (AMPAR/KAR) antagonist DNQX (100 μM) and recorded I_{inh} from OFF GCs. Under this condition, rod signals were propagated to OFF GCs by the rod→cone pathway, which does not rely on AMPAR/KARs (Figure 1) (Manookin et al., 2008; Münch et al., 2009; Pang et al., 2007; Murphy and Rieke, 2008). DNQX strongly suppressed OFF cell I_{inh} (Figures 2A and 2B). With DNQX, a 100 R*/rod/s background reduced sensitivity by only ~2-fold, consistent with adaptation at the level of rods (Dunn et al., 2006). Thus, the much larger (>20-fold) reduction in sensitivity induced by background light under control conditions cannot be explained by a mechanism resident to the rod→cone pathway.

Our interpretation of these results relies in part on the exclusion of direct cone stimulation by green light in the ventral retina, where cones primarily express a UV-sensitive opsin (Applebury et al., 2000; Nikonov et al., 2006; Szél and Röhlich, 1992; Wang et al., 2011). To confirm this, we measured rod- and cone-mediated GC responses to 200 ms flashes of either green or UV light in the ventral retina from mice with genetic mutations in either rod or cone transducin genes: Gnat1$^{-/-}$ mice in which rod signaling is abolished (Calvert et al., 2000), and Gnat2$^{-/-}$ (Gnat2^{cpfl3}) mice in which cone signaling is abolished (Chang et al., 2006) (Figure 2D).

Rod-mediated responses in Gnat2$^{-/-}$ cells were ~5.6-fold more sensitive to green than to UV light, consistent with rhodopsin's spectral sensitivity. Cone-mediated responses in Gnat1$^{-/-}$ cells were ~23-fold more sensitive to UV than to green light, consistent with the dominant expression of UV-sensitive opsin in cones of ventral retina (Naarendorp et al., 2010; Wang et al., 2011). Notably, cone-mediated Gnat1$^{-/-}$ responses to green stimuli were ~4 log units less sensitive than rod-mediated Gnat2$^{-/-}$ responses to the same stimuli (Figure 2E) (Naarendorp et al., 2010). Hence, the levels of green light stimulation used throughout this study (<−0.33 $\log_{10}$ nW/mm^2, equivalent to ~600 R*/rod/s) almost exclusively activated rods (Figure 2E).

The RB Pathway Encodes Michelson Contrast at Backgrounds where Event Detection Is Suppressed

The analysis above supports the accepted notion that RB synapses lose function in background light. But the experiments above, like previous ones, tested sensitivity using transient light increments (i.e., Weber contrast) rather than fluctuations around a mean (i.e., Michelson contrast) (Dunn et al., 2006; Oesch and Diamond, 2011). Therefore, we examined RB pathway-mediated

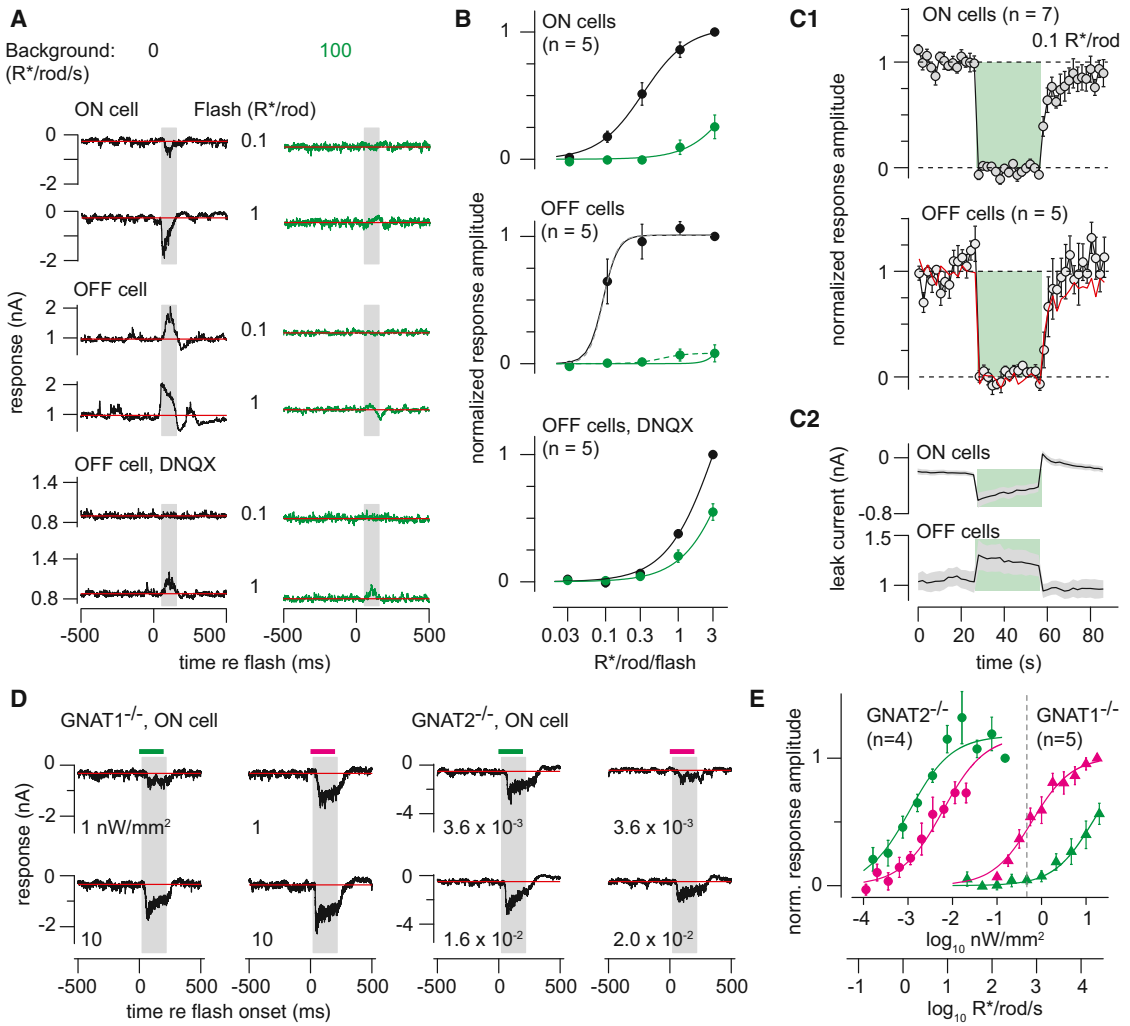

Figure 2. Background Light Suppresses Rod-Mediated Flash Responses

(A) Ten millisecond flashes (at time 0) evoking 0.1 or 1 R*/rod (green light, 0.3 mm diameter) were presented on darkness or added to a background (100 R*/rod/s). Responses were measured in ON or OFF ganglion cells; OFF responses also were recorded in DNQX (100 μM). V_{hold} = −70 mV (ON cells) or 0 mV (OFF cells; 10 kHz sampling; 2 or 4 kHz Bessel filtering). Amplitudes were measured in a window 50–125 ms after flash onset (shaded region) after subtracting the baseline current (red line, measured over 500 ms prior to flash).

(B) Intensity-response functions for flashes presented on darkness (black) or background (green). Responses were normalized to the response to the brightest flash from darkness before averaging across cells. Error bars, ±SEM. Lines show fitted sigmoidal equations that share amplitude (A) and exponent (q) values but have unique half-saturation constants (σ). ON cell parameters: A = 1.0, σ_{dark} = 0.31, $\sigma_{background}$ = 6.5, q = 1.4; OFF cell parameters: A = 1.0, σ_{dark} = 0.088, $\sigma_{background}$ = 5.3, q = 4.2; OFF cell in DNQX parameters: A = 2.2, σ_{dark} = 3.5, $\sigma_{background}$ = 7.0, q = 1.3. OFF cell data with the background were better captured by an independent fit (dashed line): A = 0.082, $\sigma_{background}$ = 0.56, q = 2.6.

(C1) Background-subtracted responses to flashes (0.1 R*/rod, 1-mm-diameter spot) before, during, and after presentation of a background (100 R*/rod/s) for 30 s (green region). Responses were normalized to the average flash response before the background presentation.

(C2) Baseline currents measured between the flash responses for the data in (C1).

(D) Responses to flashes of either green or UV light (200 ms, 1-mm-diameter spot) presented on darkness in mice lacking either rod ($Gnat1^{-/-}$) or cone ($Gnat2^{-/-}$) function. Intensity is indicated below each trace (nW/mm^2). Background-subtracted responses were measured over a window 20–220 ms after flash onset.

(E) Intensity-response functions for data in (D). Responses were normalized across cells before averaging by dividing by the response to the brightest green stimulus ($Gnat2^{-/-}$; n = 2 ON cells, 2 OFF cells) or UV stimulus ($Gnat1^{-/-}$; n = 5 ON cells). Error bars, ±SEM across cells. $Gnat2^{-/-}$ parameters: A = 1.2, σ_{green} = 0.0011, σ_{UV} = 0.0061, q = 0.92; $Gnat1^{-/-}$ parameters: A = 1.0, σ_{green} = 14.3, σ_{UV} = 0.61, q = 0.98. Dashed vertical line indicates the brightest green light used in the remainder of this study (−0.33 $\log_{10}$ nW/mm^2, equivalent to ~600 R*/rod/s). Green light at this intensity did not elicit significant cone-mediated responses in the $Gnat1^{-/-}$ mice.

responses to contrast modulated at a low temporal frequency around the mean luminance (1 Hz, 100% contrast modulation; Figures 3A1 and 3A2). In some experiments, a 1.0-mm-diameter spot was presented at means of 1–128 R*/rod/s; in others, a 0.3-mm-diameter spot was presented at means of 2–256 R*/rod/s. Both ON cell I_{exc} and OFF cell I_{inh} were modulated at

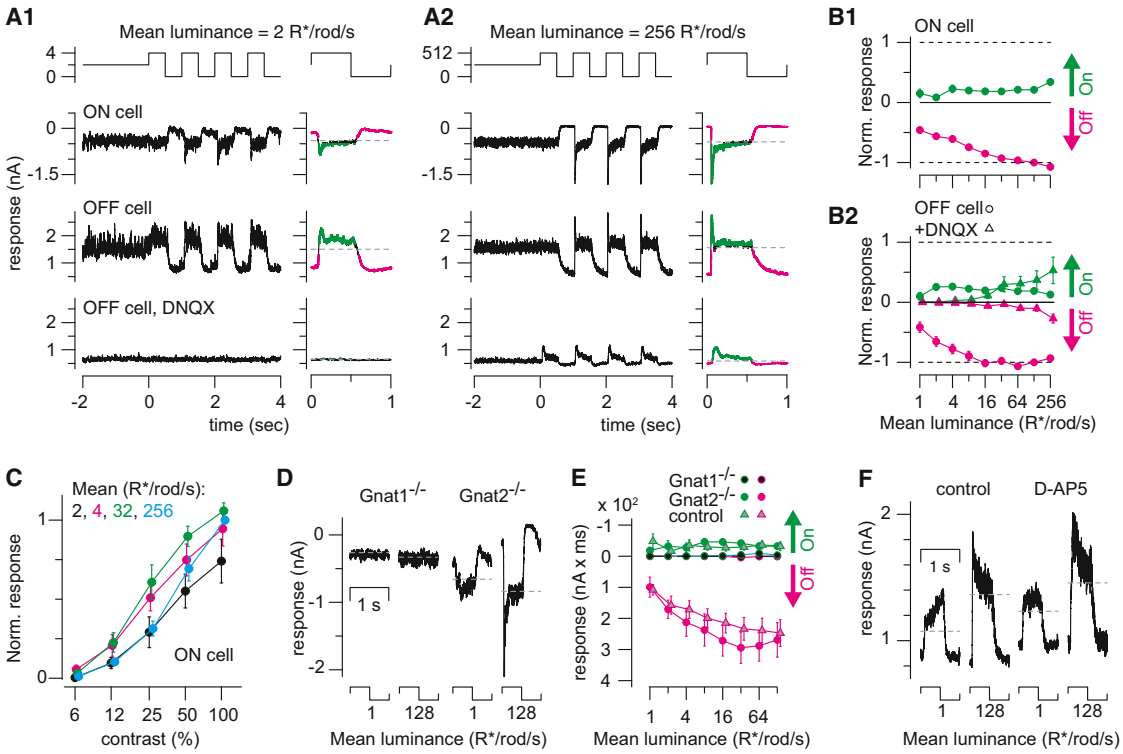

Figure 3. Ganglion Cell Responses to Michelson Contrast Depend on the Rod→Rod Bipolar Cell Pathway

(A1) Responses to contrast modulation (100% contrast, 1 Hz) at a background of 2 R*/rod/s. Responses are shown for an ON GC and for an OFF GC in control conditions and in the presence of DNQX (100 μM). At right: averaged responses (average of nine cycles, excluding the first). On responses (green) and Off responses (magenta) are represented as points >1 SD of the baseline current (measured over 2 s before contrast onset). V_{hold} = −70 mV (ON cells) or 0 mV (OFF cells; 10 kHz sampling; 2 or 4 kHz Bessell filtering).

(A2) Same format and cells shown in (A1) at a higher mean background. Averages of four cycles (excluding the first) are shown to the right of raw data.

(B1) Averaged On and Off integrated responses from ON cells, normalized to the Off response at the 128 R*/rod/s background and multiplied by −1 to generate the same sign as for OFF cells in (B2). Data include seven cells recorded at 1–128 R*/rod/s (1-mm-diameter spot) and five cells recorded at 2–256 R*/rod/s (0.3-mm-diameter spot). Error bars, ±SEM across cells.

(B2) Same format as (B1) for OFF cells. Data for both control and DNQX conditions were normalized to the control response at the 128 R*/rod/s mean. Control data include 11 cells recorded at 1–128 R*/rod/s (1-mm-diameter spot) and five cells recorded at 2–256 R*/rod/s (0.3-mm-diameter spot). DNQX data include five cells recorded at levels 1–128 R*/rod/s (1-mm-diameter spot) and four cells recorded at 2–256 R*/rod/s (0.3-mm-diameter spot).

(C) Responses to a number of contrast levels were observed across the range of backgrounds studied. A peak-to-peak response was calculated, from amplitudes measured as in (B1), and normalized to the 100% contrast response at the 256 R*/rod/s mean, before averaging across cells (n = 5; 0.3-mm-diameter spot). Error bars, ±SEM across cells.

(D) Average responses to one cycle of contrast modulation at means of either 1 or 128 R*/rod/s for ON cells in either Gnat1$^{-/-}$ or Gnat2$^{-/-}$ mice.

(E) On and Off integrated responses (nA × ms) for ON cells in Gnat1$^{-/-}$ (n = 5) and Gnat2$^{-/-}$ mice (n = 5) and control cells (n = 7) recorded with the same stimulus (1 mm diameter). Integrated inward currents (On responses) are plotted upward and outward currents (Off responses) are plotted downward to match the conventions in part (B).

(F) OFF cell's inhibitory currents recorded at two mean potentials under control conditions and in the presence of D-AP5 (100 μM).

all backgrounds, and results from the two experiments were similar and were combined in a population analysis (Figures 3B1 and 3B2).

Responses to light increments (On responses) included sustained components that were similar in amplitude at each background and transient components that emerged at higher mean backgrounds (Figures 3A1, 3A2, 3B1, and 3B2). Notably, currents in both ON (n = 12) and OFF (n = 16) GCs were modulated more strongly by decrements (Off responses) than by increments in light intensity: backgrounds appeared to set a tonic current that was reduced substantially at light Off. We quantified the On and Off responses by averaging the response cycles at each mean luminance and integrating the currents >1 SD above or below the baseline (measured over the 2 s before contrast modulation). For ON cells, On responses were inward (negative) currents and Off responses were outward (positive) currents; the opposite was true for OFF cells (Figures 3A1 and 3A2). After normalizing the data to the Off response at the 128 R*/rod/s mean, the Off response amplitude exceeded the On response amplitude by 3- to 7-fold at the two brightest backgrounds (Figures 3B1 and 3B2).

Next, we asked how ganglion cells respond to low contrasts at different mean backgrounds. We measured responses to a range of contrasts (6%–100%) across background intensities

from 2–256 R*/rod/s (Figure 3C). On and Off responses were quantified as in Figure 3B1, and peak-to-peak amplitudes were normalized across cells (n = 5) to the 100% contrast response at the brightest mean level (256 R*/rod/s). Contrast sensitivity was highest at intermediate levels (4, 32 R*/rod/s), but contrast response amplitudes at each of the four levels differed by less than a factor of two. Thus, contrast sensitivity depended only weakly on mean luminance within the range we considered.

Behaving mice encode contrast using rod pathways (Umino et al., 2008). To test how our recorded responses to contrast depended on the RB pathway specifically, we measured the effect of DNQX (100 μM) on I_{inh} recorded in OFF GCs (n = 9). DNQX blocked I_{inh} strongly at dim backgrounds (<16 R*/rod/s) and strongly attenuated I_{inh} at higher backgrounds (Figures 3A1, 3A2, 3B1, and 3B2). Notably, the DNQX-resistant On and Off currents were modulated almost symmetrically when compared to the control currents, which were largely Off modulated (Figure 3B2). Therefore, we conclude that under control conditions, the strong, asymmetric modulation by light decrements is mediated primarily by the RB pathway and that this pathway continues to encode Michelson contrast at backgrounds as high as 256 R*/rod/s.

Two independent experiments reinforced this conclusion. First, we confirmed that the recorded contrast responses were rod mediated. At backgrounds of 1–128 R*/rod/s (1-mm-diameter spot), the rod-mediated Gnat2$^{-/-}$ responses showed normal amplitudes (n = 5 ON GCs, Figure 3D; n = 4 OFF GCs, data not shown), but cone-mediated Gnat1$^{-/-}$ responses were largely absent (n = 5 ON GCs, Figure 3E). All of the Gnat1$^{-/-}$ GCs, however, were light-sensitive and responded to bright flashes (see Figures 2D and 2E; the cells in Figure 3D are the same as those in Figure 2D).

Second, we excluded the possibility that DNQX acted nonspecifically on NMDA receptors (NMDARs). The effect of DNQX was not mimicked by the NMDAR antagonist D-AP5 (100 μM; n = 3; Figure 3F), suggesting that DNQX acted at the RB→AII synapse, at which transmission is mediated exclusively by AMPARs (Singer and Diamond, 2003; Trexler et al., 2005), and did not cause nonspecific block of the NMDA receptors that could modulate gap junction coupling between AIIs (Kothmann et al., 2012). Also, we excluded the possibility that the responses at dim mean levels were mediated by amacrine cells, other than the AII, that might use NMDA receptors to respond to glutamate released from CBs. Thus, it appears that the DNQX-sensitive GC responses to contrast modulation arise from the rod→RB→AII pathway.

RB-AII Synapses Encode Michelson Contrast at Elevated Backgrounds

We recorded light-evoked excitatory currents (V_{hold} = −70 mV) from AIIs (n = 4 cells; Figures 4A1 and 4A2) in the whole-mount retina to test the hypothesis that the responses to Michelson contrast recorded in GCs arose from the RB pathway. Like the GC responses, these currents exhibited sustained components that were relatively constant over a range of backgrounds (2–256 R*/rod/s; 0.3-mm-diameter spot) and transient components that increased in amplitude at elevated backgrounds (Figures 4B1 and 4B2). Notably, the AIIs' currents, like the GCs', were modulated primarily by light decrements (Figures 4A1, 4A2, 4B1, and 4B2). The pattern of On and Off responses in AII currents was almost identical to that observed in OFF GC I_{inh}, which presumably reflects transmission from AIIs primarily (Figure 4B1).

To determine how the AII responses depended on input from the RB pathway, we examined the effect of DNQX (100 μM), which blocks RB→AII synapses. DNQX almost completely inhibited AIIs' responses at dim backgrounds (<16 R*/rod/s) (Figures 4A1, 4A2, 4B1, and 4B2). Like OFF GCs' I_{inh}, AIIs' currents in the presence of DNQX were smaller and modulated symmetrically by On and Off modulation around mean luminance >16 R*/rod/s (Figure 4B2). Currents were not altered substantially by the addition of D-AP5 (100 μM; n = 2; Figure 4E). Thus, the effect of DNQX was restricted to blocking AMPARs at the RB→AII synapse (Hartveit and Veruki, 1997; Trexler et al., 2005). We conclude that the RB pathway mediated the DNQX-sensitive response, including the large suppression of tonic current at light Off measured under control conditions.

We validated this conclusion in two ways. First, we established that the baseline current measured at each mean luminance prior to the contrast modulation became more positive at elevated mean levels, suggesting that tonic glutamate release from RBs was suppressed by background illumination (Figure 4C). Second, the noise (variance) of this same current was diminished over the same range of mean luminance, consistent with suppression of tonic glutamate release from RBs (Figure 4D). Consistently, the baseline currents recorded in AIIs in the presence of DNQX were reduced and their variance became small; neither amplitude nor variance changed with the mean luminance (Figures 4C and 4D). The DNQX-resistant responses are explained by rod→cone signaling by which rod signals are transmitted to AIIs via gap junctions with ON CBs (Figure 1). Notably, these electrical synapses lack the high levels of light-dependent noise inherent to the RB→AII chemical synapses. In summary, our observations are consistent with previous measurements showing suppression of transmission from RBs at the elevated backgrounds that cause RB depolarization and accompanying vesicle depletion at the RB→AII synapse (Jarsky et al., 2011; Oesch and Diamond, 2011).

To rule out that DNQX blocked inhibitory inputs to AIIs activated by CB stimulation, we assessed whether AII currents evoked by contrast modulation at the highest mean (256 R*/rod/s) exhibited inhibitory components. We made targeted whole-cell recordings from GFP-expressing AIIs in whole-mount retinas from Fbxo32-GFP mice (Cembrowski et al., 2012; Siegert et al., 2009). GFP was visualized by two-photon laser-scanning microscopy using relatively weak (5–7 mW at the level of the retina) and brief laser exposures (<10 s) that preserved responses to contrast at backgrounds of 256 R*/rod/s (Borghuis et al., 2013).

First, we changed the AIIs' V_{hold} from −70 mV (near E_{Cl^-}) to 0 mV (E_{cation}). Although AIIs' membrane potentials cannot be controlled precisely owing to the significant electrical coupling within the AII network (Pang et al., 2007), this manipulation should have enhanced any outward currents mediated by GABARs or GlyRs. This manipulation, however, reduced both

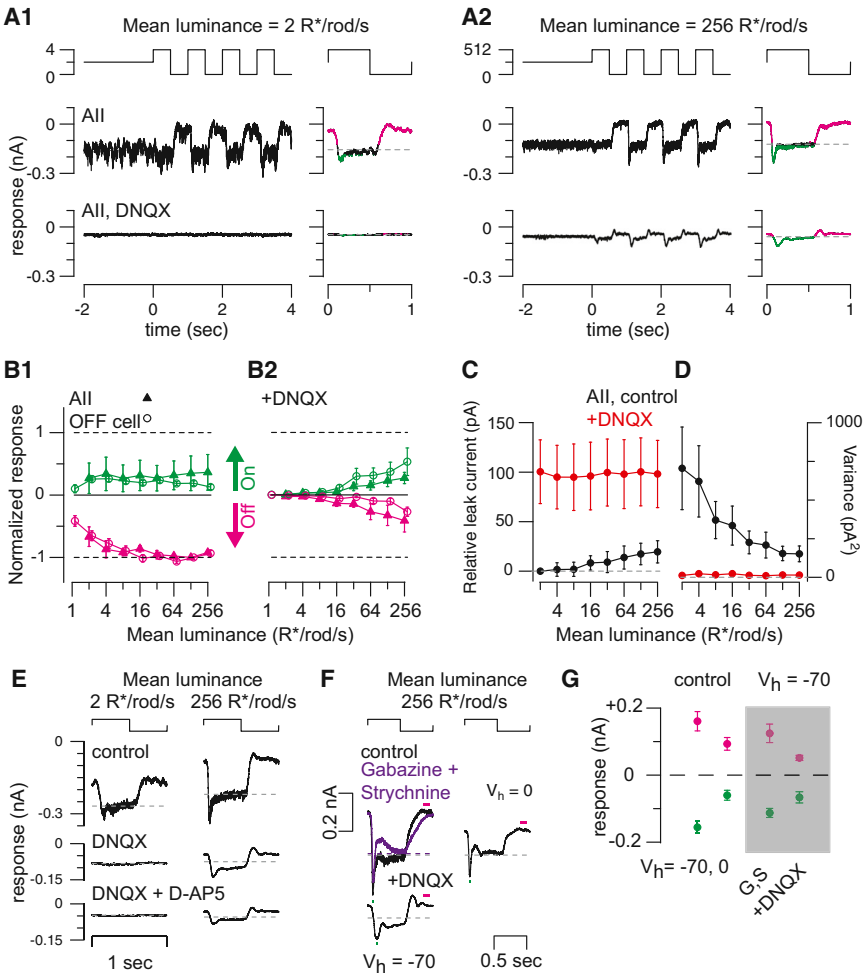

Figure 4. AII Amacrine Cell Responses to Michelson Contrast Depend on the Rod→Rod Bipolar Cell Pathway

(A1) Responses to contrast modulation (100% contrast; 1 Hz) at background = 2 R*/rod/s. Responses in control conditions and in the presence of DNQX (100 μM) are shown. At right: averaged responses to one cycle. Same conventions as in Figures 3A1 and 3A2. V_{hold} = −70 mV (10 kHz sampling; 2 kHz Bessell filtering).

(A2) Same format and cell shown in (A1) at a higher mean background.

(B1) Average On and Off integrated responses in AIIs (n = 4; 0.3-mm-diameter spot), normalized to the Off response at the 128 R*/rod/s background and multiplied by −1 to generate the same sign as in Figures 3B1 and 3B2. OFF cell responses from Figure 3B2 are shown (shifted rightward) for comparison. Error bars, ±SEM across cells.

(B2) Same format as (B1) for AII cells and OFF ganglion cells recorded in the presence of DNQX (n = 4).

(C) Baseline currents measured in AII cells (n = 4) relative to the baseline current measured under control conditions at the 2 R*/rod/s background. Error bars, ±SEM across cells.

(D) Variance measured during the baseline currents shown in (C).

(E) Average cycle responses to contrast modulation at two mean luminances in an example AII cell measured under control conditions and in the presence of DNQX (100 μM) and DNQX + D-AP5 (100 μM).

(F) Light-evoked currents are largely excitatory. Left: averaged responses to contrast modulation at the 256 R*/rod/s background were largely unaffected by blockade of postsynaptic $GABA_A$ (GABAzine, 20 μM) and GlyRs (strychnine, 2 μM; purple). Adding DNQX (100 μM) attenuated the response and made it biphasic (as in A2). Right: depolarizing the AII to E_{cation} reduced current amplitudes without affecting waveform, indicating that currents are largely excitatory and carried by cations.

(G) Summary of data illustrated in (F) for n = 4 recorded AIIs. Currents were averaged over the windows illustrated by green and red bars in (F).

inward and outward currents significantly (peak inward current from −156 ± 18 pA to −60 ± 15 pA; peak outward current from +161 ± 29 pA to +93 ± 19 pA; mean ± SEM; n = 4).

Second, we examined the effects of blocking $GABA_A$ and GlyRs with SR-95531 (Gabazine; 50 μM) and strychnine (2 μM) on light-evoked currents recorded at V_{hold} = −70mV. In the presence of these antagonists, the waveforms of contrast-modulated currents were largely unchanged and exhibited transient inward and sustained outward components (Figures 4F and 4G). Adding DNQX (100 μM) in addition to Gabazine and strychnine converted the responses to currents modulated symmetrically around the baseline. DNQX also delayed the responses' peaks (from 82.5 ± 2.4 ms to 143.8 ± 4.7 ms; mean ± SEM; n = 4). We conclude that the DNQX-sensitive component of AIIs' responses at V_{hold} = −70 mV is mediated primarily by excitatory synapses.

Temporal Features of Contrast Coding by the RB Pathway

Having established that the RB pathway encodes contrast at unexpectedly high light intensities, we next examined the temporal features of this encoding. First, to determine how periods of darkness affected subsequent responses to light, we performed a paired-pulse experiment. GCs were exposed to a background sufficient to suppress the brief flash response (100 R*/rod/s; see Figure 2) and then to two light pulses (200 R*/rod/s, 0.5 s) separated by varying intervals of darkness (30 ms to 3 s). For both ON GC I_{exc} and OFF GC I_{inh}, the responses to the second pulse increased with interpulse intervals up to ~1 s and then saturated (Figures 5A and 5D). The time constant of recovery was ~340 ms for ON GCs and ~610 ms for OFF GCs (exponential fit). The maximal response to the second pulse was about twice as large as the response to the first (Figure 5D); thus, the light response was enhanced by the period of darkness. Notably, the onset of the second response depended strongly on the interpulse interval: faster response onsets followed longer intervals (Figures 5B and 5C).

Next, we examined how the paired-pulse effect depended on the magnitude of the dark pulse. Dark pulses with variable negative contrasts were interspersed between two light pulses (200 R*/rod/s, 0.5 s) superimposed on a 100 R*/rod/s background

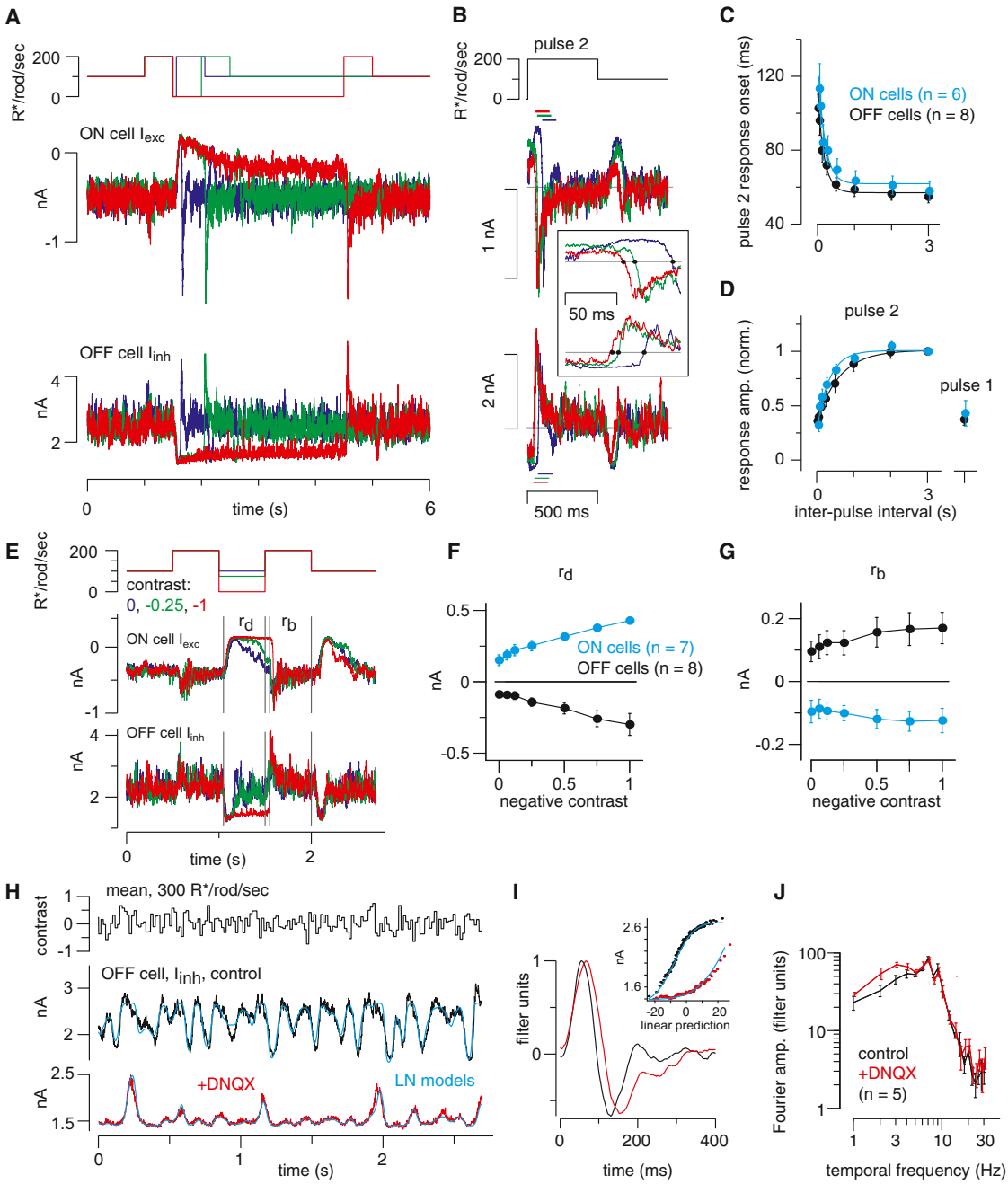

Figure 5. Periods of Darkness Facilitate Synaptic Transmission during Subsequent Responses to Light

(A) Ganglion cell responses to two light pulses (500 ms) separated by variable periods of darkness (30 ms to 3 s). The example illustrates intervals of 60, 500, and 3,000 ms (blue, green, and red). V_{hold} = −70 mV (ON cells) or 0 mV (OFF cells; 10 kHz sampling; 4 kHz Bessell filtering).

(B) Responses to the second pulse were background subtracted and aligned to pulse onset. Inset: systematic change in response onset as a function of interpulse interval; dots show the time when the response crossed the baseline (gray line). Colors indicate interpulse interval, as shown in (A). Response amplitude was quantified over a 100 ms window, starting at the time when the response crossed the baseline (thin horizontal lines).

(C) Response onset (see inset in B) became faster with longer interpulse intervals. Error bars, ±SEM across cells. Data from ON cells were shifted rightward slightly (30 ms) for visualization purposes (similar shift in part D). Fitted exponential functions are shown for ON (τ = 180 ms) and OFF (τ = 175 ms) cells.

(D) The pulse 2 response increased with interpulse interval. Responses were normalized to the response following the 3 s interpulse interval. Pulse 2 responses (leak subtracted) were measured over a 100 ms window following the determined onset time (see B, inset). The pulse 1 response was measured over a 100 ms window starting 40 ms after pulse onset. Fitted exponential functions are shown for ON (τ = 336 ms) and OFF (τ = 606 ms) cells.

(E) Different negative contrasts were interspersed between two bright pulses. Background-subtracted responses were measured within windows indicated for the response to dark pulse (r_d) and the second bright pulse (r_b).

(legend continued on next page)

(Figure 5E). The negative contrast pulse suppressed GC currents relative to baseline (i.e., outward for ON I_{exc} and inward for OFF I_{inh}) (r_d; Figure 5F). Notably, even the 0 contrast pulse (i.e., a return to the 100 R*/rod/s background; blue trace in Figure 5E) suppressed the GC currents. Furthermore, the response to the bright pulse following the negative contrast step (r_b; Figure 5G) was nearly independent of the negative contrast level. Thus, any dimming potentiated subsequent On responses.

Finally, we used white noise stimulation to examine responses over a range of temporal frequencies at a background of 300 R*/rod/s (see Experimental Procedures) (Figure 5H). Using a linear-nonlinear (LN) cascade analysis, we extracted a linear filter and a static nonlinearity (Beaudoin et al., 2008; Chichilnisky, 2001; Kim and Rieke, 2001). The filter reflects temporal processing by the presynaptic circuit and postsynaptic ligand-gated receptor channels (Figure 5I); the nonlinearity shows the relationship between the filtered stimulus and synaptic transmission to the recorded cell (Figure 5I, inset).

The LN model accurately reproduced the response to a test stimulus that was not used to generate the model (Figure 5H). The linear filter was biphasic in control conditions, reflecting band-pass frequency tuning (Figures 5I and 5J). To test the hypothesis that the filter might reflect contributions from a slow rod→RB pathway and a faster rod→cone pathway, we repeated the experiment after blocking the RB pathway with DNQX (100 μM). Counter to our expectation, the filter broadened slightly in the presence of DNQX (i.e., tuning shifted marginally to lower frequencies) (Figures 5I and 5J). Consistent with our previous results, DNQX also suppressed GC responses: the SD of the responses decreased from 257 ± 59 pA under control conditions to 80 ± 29 pA in the presence of DNQX (difference of 177 ± 36 pA, $p < 0.01$; $n = 5$). We conclude, then, that both rod→RB and rod→cone pathways exhibited similar temporal tuning under our experimental conditions and contributed similarly to the temporal bandwidths of GC responses. Thus, the band-pass tuning of the circuitry presynaptic to GCs likely originates at the photoreceptor→bipolar cell synapses (Armstrong-Gold and Rieke, 2003).

In conclusion, these experiments demonstrated that the rod→RB pathway can encode Michelson contrast at backgrounds that strongly suppress the sensitivity to brief increments. Coding contrast depends on periods of darkness (i.e., negative contrast) to enhance subsequent responses to light (i.e., positive contrast). We postulated that this process reflected the dynamics of use-dependent plasticity (i.e., depletion and recovery of the readily releasable pool [RRP] of vesicles) at RB-AII synapses. Next, we examined these dynamics directly.

Signal-to-Noise Ratio at the RB-AII Synapse Depends on Presynaptic Depolarization and Temporal Frequency Composition

Background light depolarizes RBs (Jarsky et al., 2011; Oesch and Diamond, 2011). Therefore, we studied coding at the RB→AII synapse using RB depolarization as a proxy for background light. First, we quantified the signal-to-noise ratio (SNR) of transmission as presynaptic V_M was varied between −57 and −42 mV (Figure 6A). After a 1 s period at the mean V_M, filtered Gaussian white noise (4–50 Hz range) was superimposed on the RB command potential (a 250 ms sequence repeated 20 times; SD = 6 mV). Calculated SNR (see Experimental Procedures) decreased as V_M depolarized, and the majority of the reduction occurred between −54 and −45 mV (Figure 6B; n = 8 RB-AII pairs). This finding was reproduced by a previously described phenomenological model of transmission at the RB-AII synapse (Jarsky et al., 2011) (Figure 6B). This model considers release as arising from a single cycling vesicle pool, the RRP, and the correspondence between experiments and the model indicated that the reduction in SNR arises from depletion of the RRP by tonic release at depolarized mean V_M. According to some estimates, the depolarized end of this range of V_M corresponds to background levels that evoke <20–50 R*/rod/s, and by this account the RB synapse signals over a very restricted intensity range just above visual threshold (Dunn et al., 2006; Jarsky et al., 2011; Oesch and Diamond, 2011).

Because background light modulates RB membrane noise as well as mean V_M (Dunn et al., 2006), we examined how release rate was affected by membrane noise (Figures 6C1 and 6C2). At hyperpolarized V_M, noise raised the rate of ongoing exocytosis; this effect became more pronounced as the noise variance was increased (Figures 6D and 6E). At depolarized potentials, however, noise did not affect the release rate (Figures 6D and 6E). Again, this finding was reproduced by our model of the synapse (Figure 6D), which demonstrated that noise increases the release rate only at hyperpolarized potentials, at which the RRP was not depleted by high rates of tonic exocytosis.

We considered that SNR might be affected by the temporal characteristics of RB V_M fluctuations. Therefore, we examined the SNR at lower frequency ranges that better approximated the ~10 Hz cutoff of rod-mediated responses (Figure 5J). Analysis of SNR at lower frequency ranges, however, required repeated presentations of lengthy stimulus sequences, and this was difficult to achieve with paired recordings.

To avoid these experimental constraints, we used our model to simulate postsynaptic responses to filtered (50 Hz) white noise stimuli imposed on different mean V_M. The model captured the decline in SNR observed experimentally (Figure 7A) and

(F) The response to dark (outward current in ON cells, inward current in OFF cells) increased with contrast level. Error bars, ±SEM across cells.
(G) The response to the second light pulse was nearly the same following different negative contrasts.
(H) Response to repeated white-noise stimulation (average of ten repeats) in OFF ganglion cell inhibitory currents, before and after adding DNQX to block the RB-AII synapse. Cyan lines show the fits from linear-nonlinear (LN) models.
(I) LN models in control (black) and DNQX (red) conditions. Adding DNQX caused a slight delay in the filter (normalized to a peak of one) and a reduction in the range of the nonlinearity (inset).
(J) Fourier amplitude of the normalized filters in control and DNQX conditions across cells (n = 5 OFF cells). Band-pass filtering is similar in the two conditions. Error bars, ±SEM across cells. Frequencies plotted are 1–10 Hz and even frequencies between 10 and 20 Hz; data in the DNQX condition were shifted rightward slightly for visualization purposes.

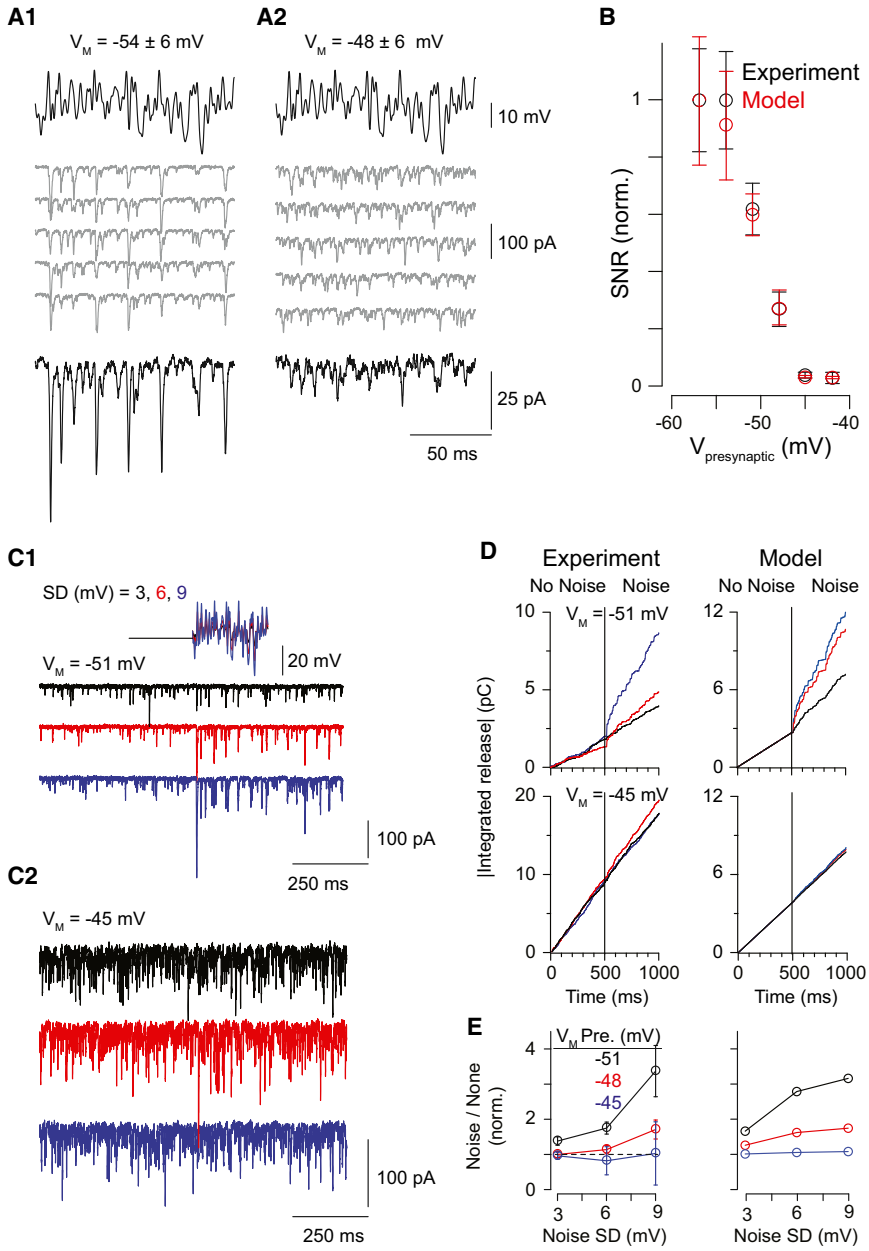

Figure 6. SNR at the RB→AII Synapse Declines with Presynaptic Depolarization

(A1 and A2) Paired recordings performed at mean presynaptic V_M = −54 mV (A1) or −48 mV (A2). Individual responses are illustrated as gray traces; the average responses are black. Note that depolarization to −48 mV increased synaptic activity uncorrelated with the stimulus (gray) and reduced the amplitude of correlated responses (i.e., the average response).

(B) Measured SNR plotted as a function of mean presynaptic V_M (black). For each cell pair, SNR was normalized to the maximum observed in that pair (error bars, ±SEM). Overlaid in red is the relationship between SNR and mean V_M predicted by a phenomenological model of synaptic transmission (error bars, ±SD).

(C1 and C2) Noise increased release at hyperpolarized potentials. Excitatory postsynaptic currents (EPSCs) recorded in AIIs when the presynaptic RB was clamped at −51 mV (C1) or −45 mV (C2) with or without noise (SD = 3, 6, or 9 mV; black, red, and blue, respectively).

(D) Noise increases release (measured as the integral of the postsynaptic current) at V_M = −51 mV but not −45 mV (left); this was predicted by the model of the synapse (right).

(E) Summary of the effect of noise on tonic release. Membrane noise enhanced release significantly at hyperpolarized potentials at which the RRP is not depleted.

indicated that the reduction in SNR arose from depletion of the readily releasable pool (RRP) of vesicles by tonic exocytosis at depolarized potentials (Figure 7B). The reduction in SNR became less pronounced as the stimulus was filtered at lower frequencies (8 and 2 Hz) (Figure 7A); this can be explained by the prolonged hyperpolarizing stimulus segments that allowed for replenishment of the RRP. Thus, the size of the functional RRP was increased when stimulus frequency is lowered (Figure 7B). This finding suggests that the low frequency of rod responses provides a mechanism for improving SNR of transmission at the RB synapse at depolarized V_M.

Interestingly, the power spectra of the simulated responses showed temporal tuning: SNR was highest at frequencies near ~10 Hz and declined at both lower and higher frequencies (Figure 7A). To explore this phenomenon further, we simulated postsynaptic responses to pure sine waves of different frequencies and observed that SNR declined at very low frequencies (Figure 7C). This decline in SNR was attributed to slow depolarizations, during which time the RRP is depleted before the depolarization is completed. Thus, at low frequencies (e.g., 2 Hz) the postsynaptic response does not track the presynaptic V_M (Figure 7D). This indicates that attenuation of low stimulus frequencies may be an inherent property of bipolar cell ribbon synapses.

The Dynamics of Transmission from RBs Permit Contrast Coding at Depolarized Membrane Potentials

Next, we examined temporal modulation of transmission at RB synapses using paired RB-AII recordings. A paired-pulse stimulus was applied at moderately depolarized V_M (−48 mV) so that release could be modulated bidirectionally. From −48 mV, the RB was depolarized briefly to a physiological level (−42 mV, 500 ms) and then hyperpolarized (−55 mV) for a variable interval (100–3,000 ms) to allow the RRP to refill before delivering a test pulse (−42 mV for 500 ms). The synaptic

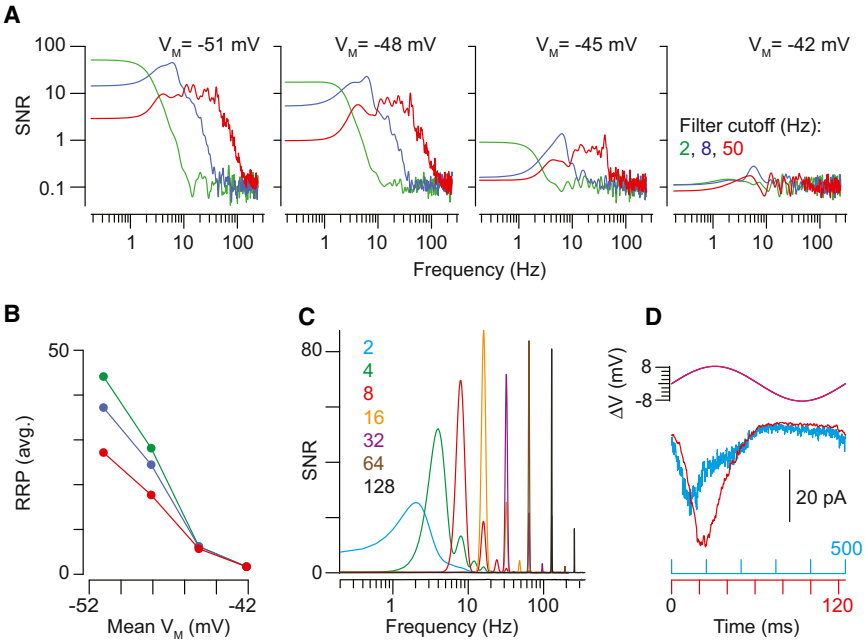

Figure 7. Assessing the Stimulus Voltage and Frequency Dependence of SNR at the RB→AII Synapse

(A) A simulation was used to probe the relationship between presynaptic V_M and the SNR of transmission. From left to right, SNR (i.e., signal power/averaged noise power) as a function of frequency at varying simulated holding potentials: the model synapse was driven with stimuli (mean V_M ± 6 mV) filtered at cutoff frequencies of 2, 8, and 50 Hz (green, blue, and red, respectively). SNR was affected by filter frequency at hyperpolarized but not depolarized V_M.

(B) Readily releasable vesicles in the simulated presynaptic pool plotted as a function of V_M: at hyperpolarized, but not depolarized, V_M, long-lasting hyperpolarizations permit recovery of the RRP. This phenomenon underlies the frequency dependence of SNR illustrated in (D).

(C) The SNR of the synapse was assessed using pure sine wave stimuli at frequencies between 2 and 128 Hz (V_M = −48 ± 6 mV). SNR increased with frequency in the 2–16 Hz range.

(D) A comparison of simulated responses to 2 and 8 Hz sine waves illustrates the mechanism underlying the increase in SNR. During a slow (2 Hz) depolarization, RRP depletion occurs before the depolarizing voltage excursion is completed (cyan). Therefore, the response is not well-correlated with the entirety of the stimulus. This is not the case for the response to the 8 Hz stimulus (red).

response to the test pulse increased with interpulse intervals up to 1.4 s (τ of fitted curve ≈900 ms; Figures 8A1, 8A2, and 8B), and the maximal response to the test pulse was 1.5-fold larger than the response to the first. The test pulse also was reduced in amplitude when noise was imposed on the mean V_M (Figures 8C1, 8C2, and 8D), indicating that variability in membrane noise might contribute to changes in RRP size at different backgrounds in combination with the mean V_M.

In summary, hyperpolarization of the RBs enhanced AIIs' responses to subsequent depolarizations. These results were similar to those observed in the light-evoked paired-pulse experiment (Figures 5A–5D and 8B) and illustrated that the RB-AII synapse is driven effectively by interspersed periods of hyperpolarization and depolarization that would occur in response to Michelson contrast.

DISCUSSION

The conventional model of rod vision proposes that the RB pathway is specialized to encode rod signals near visual threshold and ceases to function at brighter light intensities sufficient to activate the rod→cone pathway. At these intensities, the rod→cone pathway takes over the role of encoding rod signals, and it continues to do so over the majority of the rods' operating range (DeVries and Baylor, 1995; Dunn et al., 2006; Pang et al., 2007; Soucy et al., 1998; Völgyi et al., 2004). Support for this model comes from several studies that attempted to define the signal-processing roles and operating ranges of these pathways (along with a third, the rod→OFF CB pathway) by using transgenic mice in which one or more pathways were ablated genetically (Soucy et al., 1998; Deans et al., 2002; Völgyi et al., 2004; Pang et al., 2007; Arman and Sampath, 2012). But, by their design, these studies could not determine how parallel circuits might function concurrently. Here, we took an alternate approach to examine the behavior of the RB pathway throughout the operating range of rod vision under conditions in which the rod→cone pathway remained intact. We confirmed by control experiments using mice that lacked either rod ($Gnat1^{-/-}$) or cone function ($Gnat2^{-/-}$ mice) (Figures 2 and 3) that the light responses studied here in the ventral mouse retina depended almost exclusively on rod stimulation by green light.

Our experiments, which combined light-evoked recordings in GCs and AIIs with electrophysiological and computational analysis of transmission at the RB-AII synapse, call for a reevaluation of the conventional model of RB pathway function. We found that the RB pathway remained active and encoded Michelson contrast at backgrounds >250 R*/rod/s (Figures 3 and 5), even though its ability to encode transient events was diminished significantly (Figure 2). We conclude that the transition between response modes of the RB synapse depended on the effect of presynaptic V_M on the cycling of the RRP (Figures 6 and 8).

Assessing RB Pathway Function in the Intact Retinal Circuit

In a whole-mount retinal preparation that preserved all retinal circuitry and permitted selective stimulation of rods (Figure 2), we assessed rod signaling by recording light-evoked currents from AIIs and from ON and OFF alpha and OFF delta GCs. As background illumination was varied, GC ON I_{exc} and OFF I_{inh} behaved essentially identically to currents recorded in AIIs, consistent with the RB-AII network's providing a common input

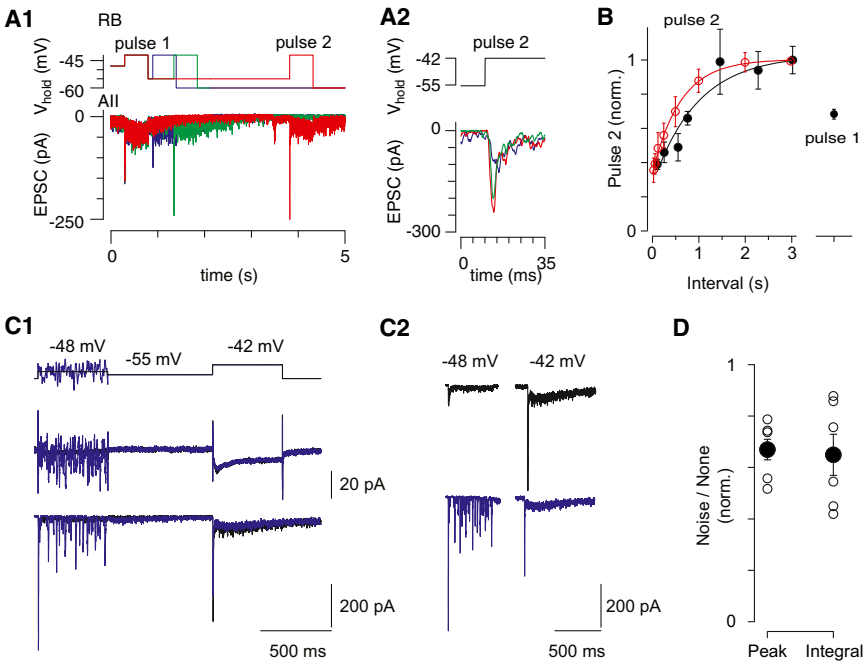

Figure 8. Hyperpolarization Enables Contrast Coding at the RB→AII Synapse

(A1) During paired recording of a coupled RB and AII, paired pulses (500 ms) to −42 mV from −48 mV, separated by a variable interval (here, 100, 550, and 3,020 ms) at −55 mV to mimic darkness, were delivered to the RB; EPSCs were recorded in the AII (n = 10 paired recordings).

(A2) The latencies of the EPSCs recorded in the AII were not dependent on the duration of the hyperpolarization.

(B) The ratio of the second response to the first (paired-pulse ratio [PPR]) increased with interpulse interval (PPR normalized to PPR at the longest interval; the time constant of the exponential fit to the data is ~900 ms). Recovery from depression is largely complete by the 1.4 s interval. Superimposed in red are the data from Figure 5D illustrating the time course of the recovery of I_{inh} recorded in OFF GCs.

(C1 and C2) Noise depresses subsequent responses to a voltage step. (C1) The RB is clamped at −48 mV without (black) and with noise (blue; SD = 9 mV) and then at −55 mV before a test pulse to −42 mV. Here, RB currents (middle traces) are not leak subtracted. The noise increased release during the first pulse, P1, thereby decreasing release evoked by the test pulse, P2. Postsynaptic currents recorded in AIIs (bottom traces) are shown again for clarity in (C2).

(D) Summary data for n = 5 paired recordings (error bars, ±SEM). The peak and the integral of the second response were decreased following the noisy prepulse (to 67% and 65% of control, peak and integral, respectively; $p < 0.05$ for both by paired t test).

to these GC types (Margolis and Detwiler, 2007; Murphy and Rieke, 2006, 2008; van Wyk et al., 2009). At all backgrounds examined, light-evoked currents recorded in AIIs and OFF GCs were largely DNQX sensitive, indicating a contribution from the RB. This is explained by the dependence of transmission at the RB→AII synapse on AMPARs (Demb and Singer, 2012; Münch et al., 2009; Singer and Diamond, 2003; Trexler et al., 2005).

From these experiments, we conclude that the RB pathway encodes Michelson contrast at backgrounds well above those at which its ability to encode transient changes in intensity (Weber contrast) is substantially diminished. Our conclusion depends upon two well-founded assumptions: one, that the only source of DNQX-sensitive input to the AII is the RB, and two, that the AII is the major conduit of rod-driven inhibitory input to OFF alpha and delta GCs. We consider each of these assumptions below.

The primary sources of glutamate in the inner retina are bipolar cell ribbon synapses (Johnson et al., 2004; Sterling and Matthews, 2005). Evidence that the RB provides the only source of ON-pathway glutamatergic synaptic input to AIIs comes from multiple EM studies, which demonstrate that virtually every ribbon-type active zone presynaptic to AIIs belongs to an identifiable RB (Strettoi et al., 1990; Tsukamoto et al., 2001; Tsukamoto and Omi, 2013). Although one study of the rabbit retina suggested that AIIs are also postsynaptic to ON CB ribbons (Anderson et al., 2011), a similar finding was not made in the mouse retina (Tsukamoto et al., 2001; Tsukamoto and Omi, 2013). Additionally, in making paired bipolar cell-AII recordings from mouse retina, we never have recorded direct chemical transmission between ON CBs and AIIs (J.-B.K. and J.H.S., unpublished data), nor has such transmission been reported in studies of the rat retina (Veruki and Hartveit, 2002) (also J.H.S., unpublished data). Finally, although AIIs do receive conventional synapses from amacrine cells in the ON sublaminae of the inner plexiform layer (Tsukamoto and Omi, 2013), and although there is a remote possibility that some of these amacrine cells are glutamatergic (Johnson et al., 2004), it is exceedingly unlikely that the vast majority of the glutamatergic, DNQX-sensitive synaptic input to AIIs that we recorded reflects anything but transmission at RB-AII synapses.

The major rod-driven inhibitory input to the OFF Alpha and Delta cells appears to be the AII. This assertion is supported by the similarity between light-evoked currents recorded in AIIs, ON alpha GCs, and OFF alpha and delta GCs over a range of background intensities (Figures 3 and 4) (Murphy and Rieke, 2006, 2008). Further, the DNQX-insensitive component of the responses recorded in OFF GCs implicates the AII as the source because AIIs receive electrical input from ON CBs via gap junctions (Figure 1). There is no experimental evidence for a bistratified amacrine cell that might convey ON CB-mediated signaling to both OFF alpha and delta GCs in a way that is DNQX insensitive.

We, however, acknowledge that the effects of DNQX on the recorded GC responses are complex. For example, many inhibitory feedback circuits are inhibited by DNQX because excitatory inputs to horizontal and amacrine cells (other than the AII) are mediated by AMPA or kainate receptors. Thus, a 75% reduction in the amplitude of the OFF GC I_{inh} (e.g., Figure 3) does not imply that the RB pathway carries 75% of the rod signal. We

interpret the response threshold under this condition (~8–16 R*/rod/s) as indicative of the threshold of the rod→cone pathway (Murphy and Rieke, 2006; Pang et al., 2007).

Contrast Coding by the RB Pathway

Our recordings of light responses from AIIs and GCs in the whole-mount preparation indicate that the RB pathway encodes temporal contrast even at backgrounds at which the rod→cone pathway is activated (Figures 3 and 4). The transition from event detection to contrast coding by the RB is enabled by the intrinsic properties of the RB-AII synapse: at backgrounds above a few tens of R*/rod/s, apparently RB V_M is depolarized to the extent that continuous exocytosis depletes the synaptic resources (i.e., releasable vesicles) necessary to encode transient signals. This is reflected in the decreased SNR of synaptic transmission evoked by a continuously fluctuating presynaptic voltage (Figure 6). The elevated release rates at depolarized V_M, however, prime the RB synapse to encode biphasic (e.g., alternating On/Off) stimuli at low temporal frequencies in a physiological range: periods of hyperpolarization elicited by negative contrast (i.e., relative darkness) allow sufficient replenishment of the vesicle pool to encode subsequent depolarization in response to positive contrast (Figures 5, 7, and 8).

Our model of RB synapse function, however, indicates that RBs at very depolarized V_M cannot encode even a slowly fluctuating stimulus that lacks substantial and long-lasting hyperpolarizations. For example, simulated SNR was low and insensitive to stimulus frequency at V_M = −42 mV (Figure 7A). This reduction is attributable to depletion of the RRP in the RB terminals by tonic exocytosis (Figure 7B), and its functional consequences are manifested by the inverse relationship between background illumination and the amplitudes and variances of tonic currents recorded in AIIs (Figures 4C and 4D).

Interestingly, temporal coding of the rod signal was similar between the RB and rod-cone circuits: the biphasic linear filter derived for the transformation of the light stimulus into the OFF GC I_{inh} was largely unaffected when signaling through the RB pathway was blocked (Figures 5I and 5J). This observation suggests that the dominant temporal filter in the retinal circuitry occurs at the photoreceptor-bipolar cell synapse (Rieke, 2001) and that this synapse acts as a band-pass filter (Armstrong-Gold and Rieke, 2003). The band-pass filtering attributable to the photoreceptor-bipolar cell synapse allows RB (and presumably other bipolar cell) synapses downstream to receive a biphasic signal. One consequence of this filtering is that suppression of synaptic transmission by negative contrast facilitates subsequent responses to positive contrast (Figures 5 and 7). Additional band-pass filtering could occur at the RB synapse or at CB synapses onto postsynaptic cells, as suggested by our model (Figures 7A and 7C).

Conclusion

We conclude that during rod vision at backgrounds >10 R*/rod/s, three complementary pathways deliver rod-driven contrast signals to OFF GCs: OFF excitation comes from both rod→OFF CB and rod→cone→OFF CB pathways (Soucy et al., 1998), and ON inhibition comes from the rod→RB→AII pathway (the current study). Two complementary pathways deliver rod-driven contrast signals to ON GCs: ON excitation comes from both rod→cone→ON CB and rod→RB→AII→ON CB pathways. Our model for rod vision suggests that parallel bipolar pathways in the retina collaborate over the majority of the rod's operating range.

EXPERIMENTAL PROCEDURES

Recordings from Retinal Whole Mounts

Ventral retinas from wild-type C57Bl/6, Gnat1$^{-/-}$, and Gnat2$^{-/-}$ mice and Fbxo32-GFP (C57Bl/6 background) (1.5–6 months old) were prepared, and recordings from ganglion and AII amacrine cells made, as described previously (Borghuis et al., 2013; Wang et al., 2011). The Animal Care and Use Committee of Yale University approved all procedures involving animal use. Retinas were superfused with Ames' medium (to which pharmacological agents were added, as noted in the text) at ~34°C. Excitatory currents were recorded near the estimated reversal potential for chloride (E_{Cl} = −67 mV), and inhibitory currents were recorded at the estimated reversal potential for cations (E_{cation} = 0 mV). Access resistances were <30 MΩ for GCs and AIIs and were compensated by 50%. In some experiments, lucifer yellow was added to the pipette solution, and morphology was visualized later in fixed tissue (Manookin et al., 2008). In other experiments, Alexa 568 hydrazide was added to the pipette solution, and cell morphology was visualized with two-photon laser-scanning microscopy immediately after recording (Borghuis et al., 2013). For AII recordings, we confirmed the bistratified morphologies and lobular appendages of the filled cells. For some ganglion cell recordings, multiple cells were recorded in the same tissue, and thus rods were not completely dark adapted.

In most experiments, light stimuli (1-mm-diameter spot) generated with a UV (370 nm peak) LED, a green (530 nm peak) LED, or the green channel of a miniature organic LED (oLED) display were projected through a 4× objective lens (Wang et al., 2011). In other experiments, light stimuli (0.3-mm-diameter spot) were presented through the condenser using a green LED. The white noise stimuli presented were programmed in MATLAB (Psychophysics Toolbox; frame rate = 60 Hz); in this case, the mean luminance of the background was equal to the mean of the spot (300 R*/rod/s). The stimulus included periods for building and validating a linear-nonlinear cascade model (Beaudoin et al., 2008; Wang et al., 2011). Photoisomerization rates were calculated based on a collecting area of 0.85 μm^2 for rods (Lyubarsky et al., 2004; Naarendorp et al., 2010; Wang et al., 2011).

Flash intensity-response functions were fit with the following equation:

$$R(I) = AI^q/(I^q + \sigma^q),$$

where I is intensity (R*/rod/s), A is the maximum response amplitude, σ is the intensity that drives a half-saturating response, and q determines the slope of the function. In Figure 2B, data were fit simultaneously to flashes on darkness or the background. The fitted curves had shared A and q parameters, but each had a unique σ. The ratio between the fitted σs determined the change in sensitivity caused by the background. The relative sensitivities to green and UV light in Gnat1$^{-/-}$ and Gnat2$^{-/-}$ ganglion cells were derived using a similar fitting routine. These curves and the fitted exponentials in Figures 5C and 5D were performed using least-squares methods in MATLAB.

Retinal Slice Recordings

Retinal slices (200 μm thick) were prepared from light-adapted, wild-type C57bl/6 mice of either sex (4–8 weeks old) as described previously (Jarsky et al., 2011). The Animal Care and Use Committee of the University of Maryland approved all procedures involving animal use. Slices were superfused with a warmed (~34°C), Carbogen-bubbled artificial cerebrospinal fluid to which blockers of $GABA_AR$-, $GABA_CR$-, GlyR-, voltage-gated Na channel-, mGluR6-regulated channel-, and Ca^{2+}-activated Cl channel-mediated currents were added (Jarsky et al., 2011). Voltage-clamp recordings were made from both RBs and AIIs (Jarsky et al., 2011). Generally, RB holding

potential was −60 mV and AII holding potential was −80 mV, and membrane potentials were corrected for junction potentials of ~−10 mV. Access resistances were <25 MΩ for RBs and <20 MΩ for AII amacrines and were compensated by 50%–90%.

Calculation of SNR

Presynaptic RBs were stimulated with filtered white noise (250 ms; Gaussian white noise filtered at 50 Hz using a first-order digital Butterworth filter implemented in Igor Pro) scaled to SD = 3, 6, or 9 mV and superimposed upon baseline depolarizations to potentials between −57 and −42 mV. A stimulus was repeated 20 times following a 2 s step depolarization during an 8-s-long trial. Trials were repeated at 60 s intervals. SNR was defined as: P_{SIGNAL}/P_{NOISE}, where P is average power measured within the 0–50 Hz bandwidth. The signal was taken as the Fourier transform of the averaged postsynaptic response to 20 repeated presynaptic stimuli, and noise was taken as the average Fourier transform of the residual difference between the average and individual postsynaptic responses (each residual was calculated in the time domain and then subjected to Fourier transform, and individual Fourier transforms were averaged).

Computational Modeling of the RB-AII Synapse

We implemented a stochastic version of our published model of the RB→AII synapse (Jarsky et al., 2011) to simulate release from and recycling of a discrete pool of available vesicles, N. This available pool obeyed the initial condition $N^0 = 80$, and the maximum number of available vesicles N_∞ obeyed $N_\infty = \text{floor}\,(N^0 \cdot h)$, where h captures Ca channel inactivation (defined in Jarsky et al., 2011). At each time step $t^k = k\Delta t$, the probability of release p_{REL} for each available vesicle was given as $p_{REL} = r(V(t^k))\Delta t$, and the probability of recycling p_{REC} for each unavailable vesicle was given as $p_{REL} = \alpha\Delta t$. Here, V is the instantaneous RB command voltage, and r, α, and Δt are used as defined previously (Jarsky et al., 2011). After calculating the vesicles to be released N^k_{REL} and the vesicles to be recycled N^k_{REC} on the k^{th} time step, the number of available vesicles at the next time step N^{k+1} was updated as $N^{k+1} = N^k - N^k_{REL} + N^k_{REC}$.

After calculating the release events for a given realization of the simulation, a delay for each event was assigned by drawing from a truncated Gaussian distribution, and an amplitude was chosen from the gamma distribution $(\Gamma(l)\Theta^l)^{-1} \cdot x^{l-1} \cdot \exp(-x \cdot \Theta^{-1})$ with shape parameter $l = 2.2$ and scale parameter $\Theta = 0.3$ (Jarsky et al., 2011).

For the simulation illustrated in Figures 6B, 6D, 6E, 7A, and 7B, on individual trials the model synapse was driven with ten repeats of a noisy 5 s stimulus at each of a range of mean voltages (V_{MEAN} = −54, −51, −48, −45 mV, all ±6 mV SD) and cutoff frequencies (f_{CUTOFF} = 2, 8, 50 Hz). For the simulation illustrated in Figures 7C and 7D, the model synapse was driven by pure sine waves 50 s in duration with cutoff frequencies from 2 to 128 Hz.

ACKNOWLEDGMENTS

Supported by EY017836 to J.H.S., by EY014454 to J.B.D., by EY021372 to H.R., W.L.K., J.B.D., and J.H.S., and by an unrestricted grant from Research to Prevent Blindness to the Department of Ophthalmology and Visual Science at Yale University. We thank J. Jiang for technical assistance.

Accepted: October 17, 2013
Published: December 26, 2013

REFERENCES

Anderson, J.R., Jones, B.W., Watt, C.B., Shaw, M.V., Yang, J.H., Demill, D., Lauritzen, J.S., Lin, Y., Rapp, K.D., Mastronarde, D., et al. (2011). Exploring the retinal connectome. Mol. Vis. *17*, 355–379.

Applebury, M.L., Antoch, M.P., Baxter, L.C., Chun, L.L., Falk, J.D., Farhangfar, F., Kage, K., Krzystolik, M.G., Lyass, L.A., and Robbins, J.T. (2000). The murine cone photoreceptor: a single cone type expresses both S and M opsins with retinal spatial patterning. Neuron *27*, 513–523.

Arman, A.C., and Sampath, A.P. (2012). Dark-adapted response threshold of OFF ganglion cells is not set by OFF bipolar cells in the mouse retina. J. Neurophysiol. *107*, 2649–2659.

Armstrong-Gold, C.E., and Rieke, F. (2003). Bandpass filtering at the rod to second-order cell synapse in salamander (Ambystoma tigrinum) retina. J. Neurosci. *23*, 3796–3806.

Beaudoin, D.L., Manookin, M.B., and Demb, J.B. (2008). Distinct expressions of contrast gain control in parallel synaptic pathways converging on a retinal ganglion cell. J. Physiol. *586*, 5487–5502.

Borghuis, B.G., Marvin, J.S., Looger, L.L., and Demb, J.B. (2013). Two-photon imaging of nonlinear glutamate release dynamics at bipolar cell synapses in the mouse retina. J. Neurosci. *33*, 10972–10985.

Calvert, P.D., Krasnoperova, N.V., Lyubarsky, A.L., Isayama, T., Nicoló, M., Kosaras, B., Wong, G., Gannon, K.S., Margolskee, R.F., Sidman, R.L., et al. (2000). Phototransduction in transgenic mice after targeted deletion of the rod transducin alpha -subunit. Proc. Natl. Acad. Sci. USA *97*, 13913–13918.

Cembrowski, M.S., Logan, S.M., Tian, M., Jia, L., Li, W., Kath, W.L., Riecke, H., and Singer, J.H. (2012). The mechanisms of repetitive spike generation in an axonless retinal interneuron. Cell Rep. *1*, 155–166.

Chang, B., Dacey, M.S., Hawes, N.L., Hitchcock, P.F., Milam, A.H., Atmaca-Sonmez, P., Nusinowitz, S., and Heckenlively, J.R. (2006). Cone photoreceptor function loss-3, a novel mouse model of achromatopsia due to a mutation in Gnat2. Invest. Ophthalmol. Vis. Sci. *47*, 5017–5021.

Chichilnisky, E.J. (2001). A simple white noise analysis of neuronal light responses. Network *12*, 199–213.

Deans, M.R., Volgyi, B., Goodenough, D.A., Bloomfield, S.A., and Paul, D.L. (2002). Connexin36 is essential for transmission of rod-mediated visual signals in the mammalian retina. Neuron *36*, 703–712.

Demb, J.B., and Singer, J.H. (2012). Intrinsic properties and functional circuitry of the AII amacrine cell. Vis. Neurosci. *29*, 51–60.

DeVries, S.H., and Baylor, D.A. (1995). An alternative pathway for signal flow from rod photoreceptors to ganglion cells in mammalian retina. Proc. Natl. Acad. Sci. USA *92*, 10658–10662.

Dunn, F.A., and Rieke, F. (2008). Single-photon absorptions evoke synaptic depression in the retina to extend the operational range of rod vision. Neuron *57*, 894–904.

Dunn, F.A., Doan, T., Sampath, A.P., and Rieke, F. (2006). Controlling the gain of rod-mediated signals in the Mammalian retina. J. Neurosci. *26*, 3959–3970.

Hartveit, E., and Veruki, M.L. (1997). AII amacrine cells express functional NMDA receptors. Neuroreport *8*, 1219–1223.

Jarsky, T., Cembrowski, M., Logan, S.M., Kath, W.L., Riecke, H., Demb, J.B., and Singer, J.H. (2011). A synaptic mechanism for retinal adaptation to luminance and contrast. J. Neurosci. *31*, 11003–11015.

Johnson, J., Sherry, D.M., Liu, X., Fremeau, R.T., Jr., Seal, R.P., Edwards, R.H., and Copenhagen, D.R. (2004). Vesicular glutamate transporter 3 expression identifies glutamatergic amacrine cells in the rodent retina. J. Comp. Neurol. *477*, 386–398.

Kim, K.J., and Rieke, F. (2001). Temporal contrast adaptation in the input and output signals of salamander retinal ganglion cells. J. Neurosci. *21*, 287–299.

Kothmann, W.W., Trexler, E.B., Whitaker, C.M., Li, W., Massey, S.C., and O'Brien, J. (2012). Nonsynaptic NMDA receptors mediate activity-dependent plasticity of gap junctional coupling in the AII amacrine cell network. J. Neurosci. *32*, 6747–6759.

Lyubarsky, A.L., Daniele, L.L., and Pugh, E.N., Jr. (2004). From candelas to photoisomerizations in the mouse eye by rhodopsin bleaching in situ and the light-rearing dependence of the major components of the mouse ERG. Vision Res. *44*, 3235–3251.

Manookin, M.B., Beaudoin, D.L., Ernst, Z.R., Flagel, L.J., and Demb, J.B. (2008). Disinhibition combines with excitation to extend the operating range of the OFF visual pathway in daylight. J. Neurosci. *28*, 4136–4150.

Margolis, D.J., and Detwiler, P.B. (2007). Different mechanisms generate maintained activity in ON and OFF retinal ganglion cells. J. Neurosci. *27*, 5994–6005.

Masland, R.H. (2012). The neuronal organization of the retina. Neuron *76*, 266–280.

Mataruga, A., Kremmer, E., and Müller, F. (2007). Type 3a and type 3b OFF cone bipolar cells provide for the alternative rod pathway in the mouse retina. J. Comp. Neurol. *502*, 1123–1137.

Münch, T.A., da Silveira, R.A., Siegert, S., Viney, T.J., Awatramani, G.B., and Roska, B. (2009). Approach sensitivity in the retina processed by a multifunctional neural circuit. Nat. Neurosci. *12*, 1308–1316.

Murphy, G.J., and Rieke, F. (2006). Network variability limits stimulus-evoked spike timing precision in retinal ganglion cells. Neuron *52*, 511–524.

Murphy, G.J., and Rieke, F. (2008). Signals and noise in an inhibitory interneuron diverge to control activity in nearby retinal ganglion cells. Nat. Neurosci. *11*, 318–326.

Naarendorp, F., Esdaille, T.M., Banden, S.M., Andrews-Labenski, J., Gross, O.P., and Pugh, E.N., Jr. (2010). Dark light, rod saturation, and the absolute and incremental sensitivity of mouse cone vision. J. Neurosci. *30*, 12495–12507.

Nikonov, S.S., Kholodenko, R., Lem, J., and Pugh, E.N., Jr. (2006). Physiological features of the S- and M-cone photoreceptors of wild-type mice from single-cell recordings. J. Gen. Physiol. *127*, 359–374.

Oesch, N.W., and Diamond, J.S. (2011). Ribbon synapses compute temporal contrast and encode luminance in retinal rod bipolar cells. Nat. Neurosci. *14*, 1555–1561.

Oesch, N.W., Kothmann, W.W., and Diamond, J.S. (2011). Illuminating synapses and circuitry in the retina. Curr. Opin. Neurobiol. *21*, 238–244.

Pang, J.J., Abd-El-Barr, M.M., Gao, F., Bramblett, D.E., Paul, D.L., and Wu, S.M. (2007). Relative contributions of rod and cone bipolar cell inputs to AII amacrine cell light responses in the mouse retina. J. Physiol. *580*, 397–410.

Protti, D.A., Flores-Herr, N., Li, W., Massey, S.C., and Wässle, H. (2005). Light signaling in scotopic conditions in the rabbit, mouse and rat retina: a physiological and anatomical study. J. Neurophysiol. *93*, 3479–3488.

Rieke, F. (2001). Temporal contrast adaptation in salamander bipolar cells. J. Neurosci. *21*, 9445–9454.

Siegert, S., Scherf, B.G., Del Punta, K., Didkovsky, N., Heintz, N., and Roska, B. (2009). Genetic address book for retinal cell types. Nat. Neurosci. *12*, 1197–1204.

Singer, J.H., and Diamond, J.S. (2003). Sustained Ca2+ entry elicits transient postsynaptic currents at a retinal ribbon synapse. J. Neurosci. *23*, 10923–10933.

Soucy, E., Wang, Y., Nirenberg, S., Nathans, J., and Meister, M. (1998). A novel signaling pathway from rod photoreceptors to ganglion cells in mammalian retina. Neuron *21*, 481–493.

Sterling, P., and Matthews, G. (2005). Structure and function of ribbon synapses. Trends Neurosci. *28*, 20–29.

Strettoi, E., Dacheux, R.F., and Raviola, E. (1990). Synaptic connections of rod bipolar cells in the inner plexiform layer of the rabbit retina. J. Comp. Neurol. *295*, 449–466.

Strettoi, E., Raviola, E., and Dacheux, R.F. (1992). Synaptic connections of the narrow-field, bistratified rod amacrine cell (AII) in the rabbit retina. J. Comp. Neurol. *325*, 152–168.

Szél, A., and Röhlich, P. (1992). Two cone types of rat retina detected by anti-visual pigment antibodies. Exp. Eye Res. *55*, 47–52.

Trexler, E.B., Li, W., and Massey, S.C. (2005). Simultaneous contribution of two rod pathways to AII amacrine and cone bipolar cell light responses. J. Neurophysiol. *93*, 1476–1485.

Tsukamoto, Y., and Omi, N. (2013). Functional allocation of synaptic contacts in microcircuits from rods via rod bipolar to AII amacrine cells in the mouse retina. J. Comp. Neurol. *521*, 3541–3555.

Tsukamoto, Y., Morigiwa, K., Ueda, M., and Sterling, P. (2001). Microcircuits for night vision in mouse retina. J. Neurosci. *21*, 8616–8623.

Umino, Y., Solessio, E., and Barlow, R.B. (2008). Speed, spatial, and temporal tuning of rod and cone vision in mouse. J. Neurosci. *28*, 189–198.

van Wyk, M., Wässle, H., and Taylor, W.R. (2009). Receptive field properties of ON- and OFF-ganglion cells in the mouse retina. Vis. Neurosci. *26*, 297–308.

Veruki, M.L., and Hartveit, E. (2002). Electrical synapses mediate signal transmission in the rod pathway of the mammalian retina. J. Neurosci. *22*, 10558–10566.

Völgyi, B., Deans, M.R., Paul, D.L., and Bloomfield, S.A. (2004). Convergence and segregation of the multiple rod pathways in mammalian retina. J. Neurosci. *24*, 11182–11192.

Wang, Y.V., Weick, M., and Demb, J.B. (2011). Spectral and temporal sensitivity of cone-mediated responses in mouse retinal ganglion cells. J. Neurosci. *31*, 7670–7681.

Wässle, H., Puller, C., Müller, F., and Haverkamp, S. (2009). Cone contacts, mosaics, and territories of bipolar cells in the mouse retina. J. Neurosci. *29*, 106–117.